07

# Experimental study of passive electrnonic components in cryogenic electronics

© D.I. Volkhin, I.L. Novikov, A.G. Vostretsov

Novosibirsk State Technical University,
630073 Novosibirsk, Russia
e-mail: d.i.volkhin@mail.ru

*Received May 5, 2025*
*Revised May 5, 2025*
*Accepted May 5, 2025*

This paper characterizes the performance of commercially available passive surface-mount devices (SMDs) — specifically capacitors and inductors in 0402 and 0201 packages — at cryogenic temperatures of 300 K, 77 K, and 4 K. The frequency dependence of their nominal values and S-parameters was measured. The results indicate that the capacitance of NPO and thin-film SMD capacitors remained within 4 % of their nominal values at both 77 K and 4 K. Their scattering matrices also exhibited only minor deviations from manufacturer specifications at these temperatures. In contrast, capacitors fabricated without thermally stabilized ceramics were found to be unsuitable for cryogenic applications. For thin-film SMD inductors cooled to 77 K, the inductance value varied by approximately 10 %. Consequently, their manufacturer-provided scattering matrices must be adjusted when designing microwave circuits for cryogenic operation. However, upon cooling to 4 K, the influence of parasitic effects from the input and output lines became significant. This interference precluded the accurate extraction of component parameters using the chosen measurement technique. Therefore, further investigation is required to fully understand the behavior of surface-mount inductors at liquid helium temperatures.

**Keywords:** capacitors, inductors, passive components, cryogenic electronics, capacitor scattering matrix, inductance scattering matrix.

DOI: 10.61011/TP.2025.09.61847.104-25

## Introduction

This study concerns cryogenic electronics employed in readout systems for superconducting quantum devices such as superconducting interference sensors (SQUIDs), bolometers, and single-photon detectors [1–5]. Quantum computer technologies based on microwave superconducting structures also require readout electronics operating at low temperatures of the order of 4 K. Cryogenic electronic systems for monitoring, controlling, and recording signals at low temperatures incorporate active semiconductor components like transistors, as well as passive elements such as resistors, capacitors, and inductors. These passive components are essential both for biasing the active components and for constructing various circuits, including attenuators and filters [6–8]. Since manufacturers do not specify the performance of commercial off-the-shelf (COTS) electronic components at temperatures below 213 K (−60 °C), their behavior in this regime constitutes a key area of research [9–12].

This paper presents the results of our research into the characteristics of commercially available passive components (capacitors and surface-mounted inductors) at 300 K, 77 K and 4 K. These components are intended for use in various electronic devices that comprise modern cryogenic measurement systems. Measurements of resistor characteristics at cryogenic temperatures were performed by the authors earlier and are presented in [13].

Surface-mounted capacitors and inductors in sizes 0402 ($1.0 \times 0.5 \times 0.5$ mm (L × W × H)) and 0201 ($0.6 \times 0.3 \times 0.3$ mm (D × W × H)) were selected in this paper as passive components. The frequency dependences of the nominal values and the parameters of the scattering matrix were measured, since in a wide frequency range, as these components are intended for use in both low-frequency and ultra-high-frequency (UHF) cryogenic electronic devices.

## 1. Passive components, equipment and measurement scheme

Surface-mounted capacitors from manufacturers including Kemet, Murata, and Kyocera AVX were selected for the study. All of them are listed in Table 1, where abbreviated series designations used in the paper are provided. The case size of Kemet capacitors is 0402, while AVX and Murata capacitors are 0201. Kemet and Murata capacitors had the same type of NPO/COG dielectric, with the exception of the Murata GRM capacitor with a nominal value of 120 pF with an X7R dielectric. Kyocera AVX capacitors are manufactured using special thin-film technology using pure metals as electrodes and a thin dielectric $SiO_2$/SiNO applied by plasma deposition. This technology ensures low losses, high dielectric constant and dielectric resistance in a wide range of high and ultrahigh frequencies, as well as a low temperature capacitance coefficient ($TCC$), comparable

**Table 1.** List of studied surface-mounted capacitors and inductors

| Element name | Manufacturer/series | Nominal values, pF/nH | Abbreviated name |
|---|---|---|---|
| Capacitors | Kemet/ CBR04 | 1; 10; 100 | CBR [15] |
| | Kyocera AVX/ Accu-P | 1; 10 | AP [14] |
| | Murata/ GJM0335 | 1; 10; 30 | GJM [16] |
| | Murata/ GRM0335 | 1; 10; 33; 120 | GRM [17] |
| Inductance | Murata/ LQP03TN | 10 | TN [18] |
| | Murata/ LQP03HQ | 10 | HQ [19] |

to the *TCC* of capacitors based on thermally stabilized NPO ceramics [14].

Surface-mounted Murata components in 0201 size were selected as inductors, produced by photolithographic thin-film technology. Such components are widely used in matching and resonant circuits of UHF devices that require miniaturization, minimal inductance deviation, and precise calibration of inductance values. The inductors of two series — LQP03TN and LQP03HQ, presented in Table 1, were selected for the study. The LQP03HQ series is characterized by an increased Q-factor, lower DC resistance, and higher self-resonant frequency.

The choice of elements is attributable to their use in broadband low-noise cryogenic UHF amplifiers [8,20,21]. In matching circuits, the deviation of the nominal value of the element from the value used in the design affects the resulting characteristics of the amplifier. The values of the elements, on one hand, are close to the maximum values used in UHF matching circuits up to 12 GHz, and on the other hand, they are close to the minimum possible for measurement in modern cryogenic equipment.

The frequency characteristics and scattering matrices of the studied passive components were measured at 300 K, 77 K, and 4 K.

The scattering matrix (S-matrix) contains complex reflection and transmission coefficients and characterizes the high-frequency properties of the measured devices. For passive elements, the S-matrix contains information about the nominal value, resonances and parasitic components, such as $ESR$, $ESL$ (for capacitors), and $C_p$ (for inductors).

For capacitors, the frequency dependence of the electrical capacitance and the dielectric loss tangent were measured in the frequency range from 100 kHz to 2 MHz, and the scattering matrix in the frequency range from 10 MHz to 10 GHz. For inductors, the frequency dependence of inductance and Q-factor were measured in the frequency range from 100 kHz to 2 MHz, and the scattering matrix in the frequency range from 10 MHz to 10 GHz. The scattering matrices were measured by sequentially connecting the elements to a 50-Ohm transmission line.

The instruments employed in the research consisted of:

• Tonghui precision LCR meter TN-2840V. Performs measurements in DC mode, as well as in the frequency band from 20 Hz to 2 MHz. Measurement method — 4-wire Kelvin method with pre-calibration.

Accessories: TN26011VS — four-wire cable with insulated clamps; TN26009V — four-wire cable with insulated tweezers.

• Vector network analyzer (VNA) Rhode&Schwarz ZVL-13. Performs measurements of complex transmission and reflection coefficients in the frequency band from 5 kHz to 13 GHz.

• Closed-cycle pulse-tube refrigerator Entropy He7.

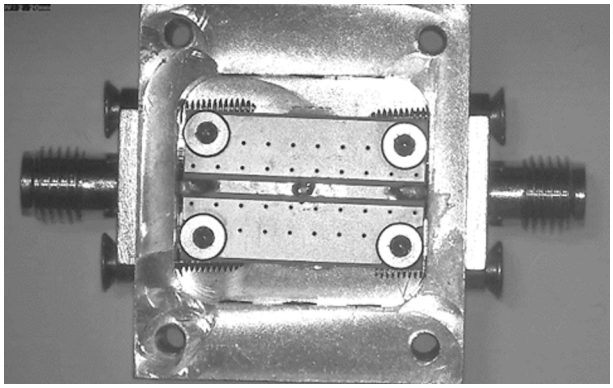

**Figure 1.** Photo of the sample holder.

A sample holder consisting of a brass housing; a Rogers 4350B printed circuit board with microstrip coplanar 50 Ω transmission lines, between which the sample was soldered; connectors SubMiniature version A (SMA) for connecting coaxial cables was used (Fig. 1). Capacitors were directly soldered to the coplanar lines to minimize losses during propagation of the UHF signal in the sample holder. Parameters of the printed circuit board and coplanar line: relative permittivity 3.66, board thickness 0.508 mm, copper foil thickness 0.018 mm, resistivity of conductors relative to resistivity of gold 0.72, the dielectric loss tangent of the board is 0.0022, the width of the coplanar line is 1 mm, the length of the coplanar line is 7.2 mm, the width of the gap between the line and the common polygon is 0.48 mm.

Additional accessories:

• Coaxial cables, length 30 cm. Used in measurements of characteristics at room temperature and at 77 K to immerse the sample holder in liquid nitrogen.

• Coaxial cables, length 150 cm. Used in measurements of characteristics at 4 K for connecting measuring instruments to the 300 K flange of the Entropy He7 refrigerator.

• Tonghui precision LCR meterTN-2840V. Performs measurements on direct current, as well as in the frequency band from 20 Hz to 2 MHz. Measurement method — 4-wired Kelvin method with pre-calibration. Accessories: TN26011VS — four-wire cable with insulated clamps; TN26009V — four-wire cable with insulated tweezers;

• Vector network analyzer (VNA) Rhode&Schwarz ZVL-13. Performs measurements of complex transmission and reflection coefficients in the frequency band from 5 kHz to 13 GHz;

• closed-cycle refrigerator with mechanical drive Entropy He7.

In the measurement process, a sample holder was used (Fig. 1), consisting of a brass housing; a Rogers 4350B printed circuit board with microstrip coplanar transmission lines made on it, with a wave resistance of 50 Ω, between which the sample was soldered; connectors SubMiniature version A (SMA) for connecting coaxial cables. Capacitors were directly soldered to the coplanar lines to minimize losses during propagation of the VHF signal in the sample holder. Parameters of the printed circuit board and coplanar line: relative permittivity 3.66, board thickness 0.508 mm, copper foil thickness 0.018 mm, resistivity of conductors relative to resistivity of gold 0.72, the tangent of the dielectric loss angle of the board is 0.0022, the width of the coplanar line is 1 mm, the length of the coplanar line is 7.2 mm, the width of the gap between the line and the common polygon is 0.48 mm.

Additional accessories:

• Coaxial cables, length 30 cm. They were used in measurements of characteristics at room temperature and at 77 K to immerse the sample holder in liquid nitrogen.

• Coaxial cables, length 150 cm. They were used in measurements of characteristics at 4 K for connecting measuring instruments to the 300 K flange of the Entropy He7 refrigerator.

• Vessel with liquid nitrogen. Used to maintain a temperature of 77 K during measurements.

The schemes of our measurements at temperatures of 300, 77, 4 K are shown in Fig. 2.

Before measurements, the following calibration procedures were used: 1) For frequency dependence measurements using the Tonghui TN-2840V LCR meter — Open/Short calibration to the sample holder plane. 2) For scattering matrix measurements using the ZVL-13 vector network analyzer — TOSM (Through/Open/Short/Match) type calibration using built-in calibration tools and calibration kit. Before measurements in the He7 refrigerator, calibration was performed as follows: 1) For frequency dependence measurements using the Tonghui TN-2840V LCR meter — Open/Short calibration on connectors at 300 K flange of the refrigerator. 2) For scattering matrix measurements using the ZVL-13 vector network analyzer — TOSM type calibration using built-in calibration tools and calibration kit at 300 K on the plane of the sample holder installed in the refrigerator.

## 2. Results

### 2.1. Frequency dependence of electrical capacitance and the dielectric loss tangent in the frequency range from 100 kHz to 2 MHz

The nominal and measured capacitance values at 300 K, 77 K, and 4 K are listed in Table 2. The capacitance values and dielectric loss tangent are the mean values obtained in the frequency range of 50−250 kHz from their frequency dependence at 300 K, 77 K and 4 K. The deviation of the capacitance values is calculated for the measurement results at 77 K and 4 K relative to the capacitance value at 300 K according to the following expression:

$$\Delta = \frac{|\overline{C_{300}} - \overline{C_T}|}{\overline{C_{300}}} \cdot 100\,\%,$$

where $\overline{C_T}$ is the mean capacitance value at temperature $T$, $\overline{C_{300}}$ is the mean capacitance value at 300 K.

The equivalent series resistance of $ESR$ of capacitors at a frequency of 100 kHz, showing the effect of parasitic components, was calculated using the following equation:

$$ESR = \frac{\overline{\mathrm{tg}\,\delta}}{\omega \overline{C_T}},$$

where $\overline{\mathrm{tg}\,\delta}$ is the mean value of the deilectric loss tangent of the capacitor, $\omega$ is the angular frequency.

The nominal and measured mean values of the capacitance, the dielectric loss tangent, and the equivalent series resistance of capacitors at a frequency of 100 kHz at 300 K, 77 K, and 4 K are listed in Table 3. The deviation of the capacitance value at 4 K and the equivalent series resistance of the capacitors are calculated relative to the capacitance value and $ESR$ measured in a refrigerator at 300 K. The values of capacitance and $ESR$, measured in a refrigerator at 300 K, are listed in the Table 3 separated by slashes.

According to the results obtained, the capacitance value did not change significantly when cooled to 4 K. The exception is the Murata GRM 120 pF sample, which does not contain a thermally stabilized ceramic substrate. This sample showed a significant decrease in capacitance with a deviation of more than 98 % from the value measured at room temperature. Notably, AVX capacitors manufactured using thin-film technology showed preservation of capacitance at cryogenic temperatures. These results suggest that not only capacitors with NPO dielectric, but also multilayer capacitors made using thin-film technology, are suitable for use at cryogenic temperatures. The equivalent series resistance, as a parameter sensitive to the magnitude of the dielectric leakage current of the capacitors [11], showed a difference in the behavior of AVX capacitors from NPO type capacitors given earlier in [11]. In conclusion, we would like to note that the value of the dielectric loss tangent

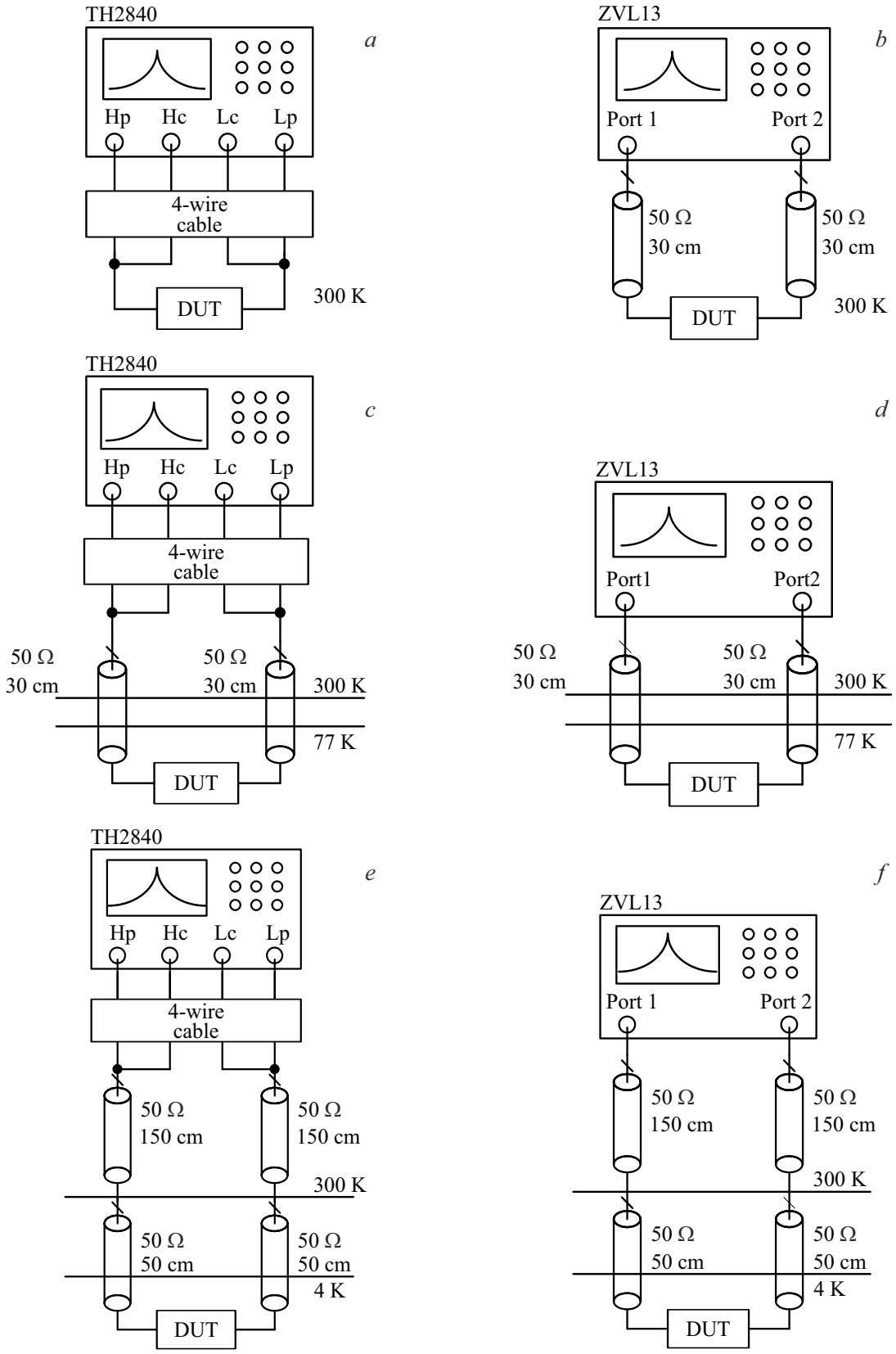


**Figure 2.** Measurement schemes: frequency dependence (*a*, *c*, *e*); scattering matrices (*b*, *d*, *f*) at temperatures of 300, 77 and 4 K. DUT — device under test.

**Table 2.** Mean capacitance values at different temperatures

| Abbreviated name | Nominal value, pF | $\overline{C}$, 300 K | $\overline{C}$, pF 77 K | $\Delta_{77K}$, % | $\overline{C}$, pF 4 K | $\Delta_{4K}$, % |
|---|---|---|---|---|---|---|
| CBR | 1 | 1.028 | 1.055 | 2.65 | – | – |
| | 10 | 9.94/9.01 | 9.74 | 2.05 | 9.19 | 0.61 |
| | 100 | 96.08 | 96.64 | 0.58 | – | – |
| ACCU | 1 | 1.021 | 1.028 | 0.7 | – | – |
| | 10 | 10.09/9.496 | 10.04 | 0.55 | 9.44 | 3.3 |
| GJM | 1 | 0.99 | 1.013 | 2.4 | – | – |
| | 10 | 10.14/9.31 | 10.17 | 0.28 | 9.44 | 1.45 |
| | 30 | 29.84 | 29.87 | 0.11 | – | – |
| GRM | 1 | 1.01 | 1.04 | 2.75 | – | – |
| | 10 | 9.98/8.8 | 10.04 | 0.6 | 9.06 | 3 |
| | 33 | 34.08/29 | 34.29 | 0.61 | 30.12 | 3.9 |
| | 120 | 115.57/97.12 | 29.56 | 74.4 | 1.59 | 98.4 |

**Table 3.** Mean values of the capacitor dielectric loss tangent and *ESR* at 100 kHz across various temperatures

| Abbreviated name | Nominal value, pF | $\overline{\mathrm{tg}\,\delta}$, $10^{-3}$ 300 K | $\overline{\mathrm{tg}\,\delta}$, $10^{-3}$ 77 K | $\overline{\mathrm{tg}\,\delta}$, $10^{-3}$ 4 K | *ESR*, Ω 300 K | *ESR*, Ω 77 K | *ESR*, Ω 4 K |
|---|---|---|---|---|---|---|---|
| CBR | 1 | 107.14 | 53.15 | – | 166023 | 80237 | – |
| | 10 | 56.12 | 49.82 | 66.91 | 8988/11299 | 8147 | 11591 |
| | 100 | 2.62 | 2.02 | – | 43 | 33 | – |
| ACCU | 1 | 83.53 | 53.73 | – | 130280 | 83219 | – |
| | 10 | 53.12 | 50.63 | 63.45 | 8377/10547 | 8028 | 10698 |
| GJM | 1 | 81.31 | 53.34 | – | 130928 | 83879 | – |
| | 10 | 53.69 | 50.85 | 63.97 | 8434/11593 | 7966 | 10785 |
| | 30 | 2.15 | 1.54 | – | 115 | 82 | – |
| GRM | 1 | 82.85 | 55.06 | – | 130337 | 84303 | – |
| | 10 | 54.95 | 51.37 | 66.06 | 8768/11010 | 8147 | 11605 |
| | 33 | 1.83 | 1.47 | 2.8 | 86/244 | 68 | 148 |
| | 120 | 15.56 | 53.95 | 19 | 214/235 | 2906 | 18980 |

for all samples changes significantly with the capacitor nominals. The reasons for this behavior remain unclear for this behavior of the dielectric loss tangent.

## 2.2. Scattering matrices of capacitors in frequency range up to 10 GHz

Scattering matrix measurements were performed on a single capacitor of each nominal value at temperatures of 300 K, 77 K, and 4 K. The matrices were measured from 10 MHz to 10 GHz after a preliminary calibration of the coaxial cables. The manufacturers provided reference scattering matrix parameters for these capacitors at 300 K, which we used for comparison with our measured data.

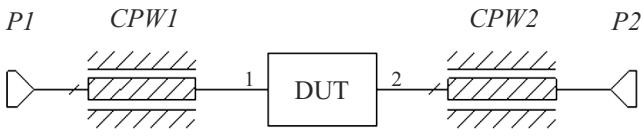


**Figure 3.** A model of the sample holder with leading coplanar lines. $P1$, $P2$ — input and output ports, $CPW1$, $CPW2$ — model of the coplanar lines of the sample holder's coplanar lines from the input and output ports, DUT — the model of the device under test.

The measured result represents the scattering matrix of a capacitor integrated into a sample holder, the model of which is depicted in Fig. 3. This sample holder model was validated by comparing its simulated S-parameters to measurements performed at room temperature. The measurements were conducted using a TOSM (Through-Open-Short-Match) calibration type with built-in calibration tools and a calibration kit.

The measured scattering matrices at 300 K, 77 K, and 4 K are presented in Fig. 4 as frequency-dependent plots of the $S11$ and $S21$ parameters. The $S22$ and $S12$ parameters exhibited a similar behavior.

To quantify the changes in the scattering matrix as a function of temperature and frequency, the parameter $\delta_{C,T}$ was calculated. This parameter is defined as the root mean square (RMS) of the relative deviation of the $S21$ parameter at temperature $T$ from its value at a reference temperature of 300 K, computed over a set of analyzed frequency points within the given range. It is calculated using the following expression:

$$\delta_{C,T} = \sqrt{\frac{1}{N-1}\sum_{k=1}^{N}\left[\left(\frac{S21_{300,k} - S21_{T,k}}{S21_{300,k}}\right)^2\right]}, \quad (1)$$

where $N$ is the total number of frequency points, $S21_{300,k}$ is the transmission coefficient at the $k$-th frequency point at 300 K, $S21_{T,k}$ is the transmission coefficient at the $k$-th frequency point at a temperature $T$.

The upper frequency limit for this analysis was set to 1 GHz. This choice was made because the influence of the sample holder on the measured scattering matrix of both capacitors and inductors becomes significant above this frequency, which would obscure the component's intrinsic behavior.

Prior to cryogenic measurements, the quality of the measurement setup was verified at 300 K by calculating $\delta_{C,300}$. This value was derived from a comparison between our measured scattering matrix and the one supplied by the manufacturer. To ensure a direct comparison, the manufacturer's data was augmented with the matrices of the coplanar transmission lines $CPW1$ and $CPW2$ (Fig. 3). The number of frequency points, $N$, was 46, corresponding to the data provided by the manufacturer, covering the range from 100 MHz to 1 GHz with a 20 MHz step.

The comparison results are presented in Table 4.

The comparison results are presented in Table 4.

The data show that for most capacitors — with the exception of the GRM 120 pF type — the deviation of the $S21$ parameter falls within a range of 0.00762 to 0.04837. This deviation shows no correlation with the measured capacitance, suggesting it may be caused by measurement error from uncontrolled variations in the system parameters during assembly and disassembly.

The change in the $S21$ parameter at 77 K relative to the room-temperature values is also shown in Table 4. The $\delta_{C,77}$ value was calculated using Equation (1) over the same frequency range (100 MHz to 1 GHz, $N = 46$ points).

**Table 4.** Values $\delta_{C,300}$ and $\delta_{C,77}$ of the relative deviation of the values of the $S21$ parameters of the scattering matrix measured at 300 and 77 K

| Abbreviated name | Nominal value, pF | $\delta_{C,300}$ | $\delta_{C,77}$ |
|---|---|---|---|
| CBR | 1 | 0.04837 | 0.03271 |
| | 10 | 0.01257 | 0.01664 |
| | 100 | 0.00762 | 0.01327 |
| ACCU | 1 | 0.0164 | 0.01371 |
| | 10 | 0.0117 | 0.01118 |
| GJM | 1 | 0.01162 | 0.014 |
| | 10 | 0.01761 | 0.01487 |
| | 30 | 0.0102 | 0.01296 |
| GRM | 1 | 0.00843 | 0.01688 |
| | 10 | 0.01483 | 0.01616 |
| | 33 | 0.01245 | 0.01507 |
| | 120 | 0.02425 | 0.07389 |

The data indicate that for most capacitors, the scattering matrix parameters at 77 K remain largely unchanged from their room-temperature values across the operational frequency range up to 1 GHz. The relative deviation of the $S21$ parameter saw a slight increase, now ranging from 0.01118 to 0.03271, but still exhibited no correlation with capacitance. This suggests that the observed deviations are not solely due to measurement error but may also be influenced by temperature-dependent changes in the measurement path and the sample itself, including alterations in the capacitance and the properties of the sample holder.

A significant deviation of the values was observed for the GRM 120 pF capacitor, which does not have a thermally stabilized ceramic substrate. For this capacitor, the relative deviation of the $S21$ parameter was 0.07389, which is significantly larger than the changes observed for other capacitors. A similar behavior can be seen when analyzing data obtained at low frequencies. According to Table 2, the deviations of the capacitance nominal value at 77 K were within 3 % for all capacitors except for the GRM 120 pF capacitor. The deviation of the GRM 120 pF nominal value at 77 K was approximately 75 %. This behavior of the $\delta_{C,77}$ mainly reflects a significant difference in the capacitance of this capacitor when it is cooled, which leads to a significant change in the frequency response of the transmission coefficient.

The quality of the scattering matrix measurements performed in the He7 refrigerator was also preliminarily evaluated at room temperature relative to the scattering matrix provided by the manufacturer. However, in order to

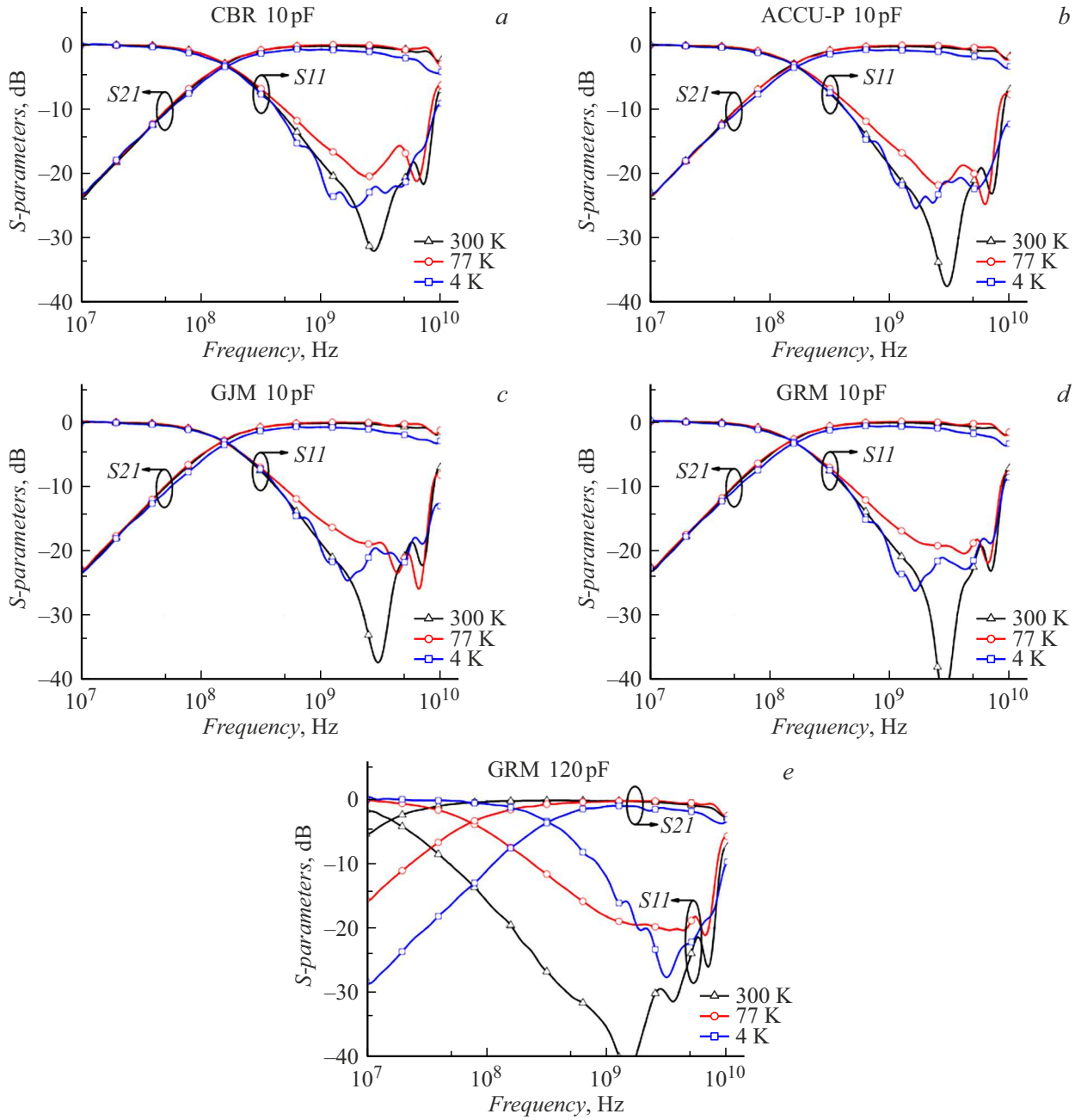


**Figure 4.** Parameters $S11$ and $S21$ of capacitor scattering matrices at temperatures of 300, 77 and 4 K; *a* — Kemet CBR04 10 pF (C0G); *b* — Kyocera AVX Accu-P 10 pF (Si/SiO); *c* — series Murata GJM0335 10 pF(C0G); *d* — Murata GRM0335 10 pF(C0G); *e* — Murata GRM0335 120 pF (X7R).

adjust the $S21$ parameters of the manufacturers' scattering matrix, we supplemented them with transmission line matrices obtained from a transmission line model that takes into account both supply coplanar lines and transmission lines of the refrigerator at a measuring temperature of 4 K. In the model, the attenuation coefficient of the transmission lines was adjusted (Fig. 5) to compensate for the difference between the $S21$ parameters of the scattering matrix provided by the manufacturer and the parameters measured in a refrigerator. The scattering matrix provided by the manufacturer was used as the model of the device under test.

The measurement quality of the scattering matrix in the refrigerator was evaluated using the value $\delta_{CR,300}$, which was obtained for two scattering matrices: measured and presented by the manufacturer. The scattering matrix provided by the manufacturer was supplemented with matrices of refrigerator transmission lines including coplanar lines of the sample holder (Fig. 5). The number of points $N$ was also 46, as provided by the manufacturer.

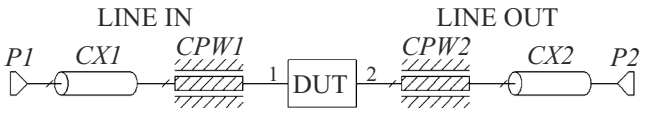


**Figure 5.** Model of refrigerator transmission lines with feeding coplanar lines of the sample holder. $P1$, $P2$ — input and output ports, LINE IN, LINE OUT — model of the refrigerator transmission line with feeding coplanar lines of the sample holder from the input and output ports, DUT — model of the device under test.

**Table 5.** Values $\delta_{CR,300}$ and $\delta_{CR,4}$ of the relative deviation of the values of the parameter $S21$ of the scattering matrix measured in a refrigerator at 300 and 4 K

| Abbreviated name | Nominal value, pF | $\delta_{CR,300}$ | $\delta_{CR,4}$ |
|---|---|---|---|
| CBR | 10 | 0.01257 | 0.06205 |
| | 100 | 0.00889 | 0.05568 |
| ACCU-P | 10 | 0.01565 | 0.06309 |
| GJM | 10 | 0.01603 | 0.06221 |
| GRM | 10 | 0.01288 | 0.05975 |
| | 33 | 0.01319 | 0.06107 |
| | 120 | 0.02449 | 0.25554 |

The comparison results are presented in Table 5.

It can be noted that the values $\delta_{CR,300}$ measured in a refrigerator at room temperature relative to the $S21$ parameters presented by the manufacturer at 300 K are in good agreement with the values $\delta_{C,300}$ measured at room temperature, obtained with calibrated coaxial lines only. A slight misalignment is most likely related to the assembly and disassembly.

The change in the $S21$ parameters at 4 K relative to the values obtained at room temperature is shown in Table 5. The value $\delta_{CR,4}$ is calculated using the Equation (1) in the range from 100 MHz to 1 GHz with 46 points.

### 2.3. Frequency dependence of inductance and Q factor in the frequency range from 100 kHz to 2 MHz

The nominal and measured values of inductance and Qfactor at 300, 77 and 4 K are shown in the Table 6 and 7. The mean values of these parameters were used as values of inductance and Q-factor, obtained in the frequency range 50−250 kHz from their frequency dependence at temperatures of 300, 77 and 4 K. The deviation of the inductance values is calculated for the measurement results at 77 and 4 K relative to the value of the inductance at 300K using the following Equation:

$$\Delta = \frac{|\overline{L_{300}} - \overline{L_T}|}{\overline{L_{300}}} \cdot 100\,\%,$$

where $\overline{L_T}$ is the mean value of inductance at temperature $T$, $\overline{L_{300}}$ is the mean value of inductance at 300 K.

The mean values of these parameters were used as values of inductance and Q-factor, obtained by measuring a set of three inductors of each type at 300 and 77 K. One sample of each type was measured at a temperature of 4 K.

Due to the fact that in the measurements at 4 K, calibration was performed on the connectors on the flange of the refrigerator at 300 K, the measurement result includes, in addition to the inductance of the measured component, the inductance of the transmission lines of the refrigerator and the sample holder. To compare the measurement results of the component at 4 K correctly, the value of the component at 300 K was measured as a reference. The inductance deviation at 4 K is calculated relative to the inductance value that was measured in the refrigerator at 300 K. The value of the inductance measured in the refrigerator at 300 K is shown in Table 6 separated by slashes. It can be seen that the parameters of the refrigerator transmission lines change significantly with cooling. This fact prevents us from measuring the inductance of the test sample at 4 K.

## 3. Inductance scattering matrix in the frequency range up to 10 GHz

The scattering matrix was measured with preliminary calibration of UHF coaxial cables in the frequency range from 10 MHz to 10 GHz. For inductors, the manufacturers provided the parameters of the scattering matrix at 300 K. These reference parameters were used to compare with our measurement results.

The obtained scattering matrix parameters for the inductors at temperatures of 300 K, 77 K, and 4 K are presented in Figure 6 as frequency-dependent plots of the $S11$ and $S21$ parameters. The parameters $S22$ and $S12$ had a similar behaviour.

To quantify the changes in the scattering matrix as a function of temperature and frequency, the value $\delta_{L,T}$ was calculated. This is the room-mean-square (RMS) value of the relative deviation of the $S21$ parameter at a temperature T from its value at the reference temperature of 300 K. The calculation was performed over 218 frequency points in the range from 1 MHz to 1 GHz:

$$\delta_{L,T} = \sqrt{\frac{1}{N-1}\sum_{k=1}^{N}\left[\left(\frac{S21_{300,k} - S21_{T,k}}{S21_{300,k}}\right)^2\right]}. \quad (2)$$

Prior to cryogenic measurements, the quality of the measurement setup was evaluated at room temperature using the parameter $\delta_{L,300}$. This value was calculated by comparing our measured scattering matrix with the one supplied by the manufacturer. To enable a direct comparison, the manufacturer's data was augmented with the matrices of the coplanar transmission lines $CPW1$ and $CPW2$ (Fig. 3), following the same procedure described

**Table 6.** Average inductance values at different temperatures

| Abbreviated name | Nominal value, nH | $\overline{L}$, nH 300 K | $\overline{L}$, nH 77 K | $\Delta_{77K}$, % | $\overline{L}$, nH 4 K | $\Delta_{4K}$, % |
|---|---|---|---|---|---|---|
| TN | 10 | 10.24/858.6 | 11.27 | 10 | 669.5 | 22 |
| HQ | 10 | 10.88/855 | 11.12 | 2.2 | 678.82 | 20.6 |

**Table 7.** Average Q-factor values at different temperatures

| Abbreviated name | Nominal value, nH | $\overline{Q}$, $10^{-3}$ 300 K | $\overline{Q}$, $10^{-3}$ 77 K | $\overline{Q}$, $10^{-3}$ 4 K |
|---|---|---|---|---|
| TN | 10 | 15.46 | 108.5 | 549.88 |
| HQ | 10 | 25.7 | 160.3 | 579.56 |

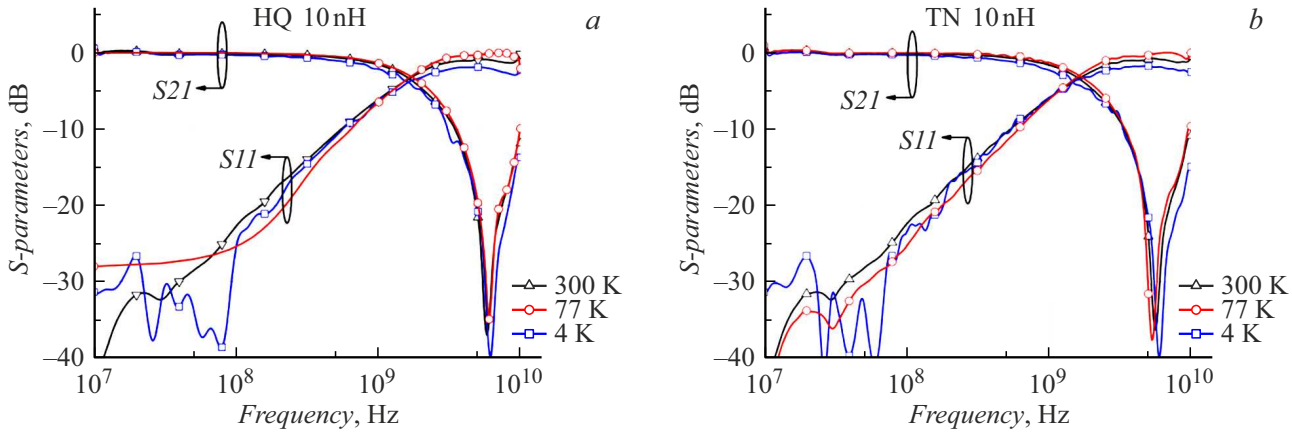


**Figure 6.** Parameters $S11$ and $S21$ of the inductance scattering matrix 10 nH at temperatures of 300, 77 and 4 K: *a* — Murata LQP03HQ; *b* — Murata LQP03TN.

**Table 8.** Values $\delta_{L,300}$ and $\delta_{L,77}$ of the relative deviation of the values of the parameter $S21$ of the inductance scattering matrix measured at 300 and 77 K

| Abbreviated name | Nominal value, nH | $\delta_{L,300}$ | $\delta_{L,77}$ |
|---|---|---|---|
| TN | 10 | 0.0061 | 0.01408 |
| HQ | 10 | 0.00511 | 0.01151 |

earlier for the capacitor measurements. The results of this comparison are presented in Table 8.

The data shows that the relative deviation of the $S21$ parameter for the inductors is 0.00511 for the HQ type and 0.0061 for the TN type. The slight discrepancy between these values is likely attributable to measurement error, possibly caused by uncontrolled variations in the measurement system parameters during its assembly and disassembly.

The change in the $S21$ parameters at 77 K, relative to their room-temperature values, is also shown in Table 8. The corresponding $\delta_{L,77}$ value was calculated using Equation (2). The data indicates that the deviation of the $S21$ parameter increased to 0.01151 for HQ and 0.01408 for TN.

This behavior suggests that the properties of both the inductors themselves and the sample holder change with temperature. This is consistent with the data in Table 6, which shows an inductance variation of approximately 10% at 77 K. This significant shift in inductance explains the corresponding increase in the variation of the $S21$ parameters compared to room temperature.

The measurement quality within the refrigerator was assessed using the parameter $\delta_{LR,300}$. This was obtained by comparing a scattering matrix measured inside the refrigerator at room temperature with the manufacturer's reference data. For this comparison, the manufacturer's matrix was supplemented with the matrices of the refrigerator's internal transmission lines, which include the coplanar lines of the sample holder (Fig. 5).

The results are provided in Table 9.

**Table 9.** Values $\delta_{LR,300}$ and $\delta_{LR,4}$ of the relative deviation of the values of the parameter $S21$ of the inductance scattering matrix measured in a refrigerator at 300 and 4 K

| Abbreviated name | Nominal value, nH | $\delta_{LR,300}$ | $\delta_{LR,4}$ |
|---|---|---|---|
| TN | 10 | 0.02244 | 0.05307 |
| HQ | 10 | 0.01869 | 0.05196 |

It is notable that the $\delta_{LR,300}$ values (0.01869 for HQ and 0.02244 for TN) are inconsistent with the earlier $\delta_{L,300}$ values obtained using only calibrated coaxial cables. The discrepancy, which is roughly an order of magnitude, is most likely due to the additional influence of the refrigerator's internal coaxial lines.

Finally, the change in the $S21$ parameters at 4 K relative to the in-refrigerator room-temperature values is shown in Table 9. The value $\delta_{LR,4}$ was calculated according to the Equation (2).

## 4. Discussion

The presented $\delta_{CR,4}$ data indicate that for most capacitors, the characteristics of the scattering matrix measured at 4 K differ from those measured at room temperature across the operating frequency range of up to 1 GHz. The deviation of the $S21$ parameter increased, falling within a range of 0.05568 to 0.06309. This suggests changes in the properties of not only the capacitors but also the sample holder and the refrigerator's input/output lines. According to Table 2, the deviation in the nominal capacitance values at 4 K did not exceed 4 %, indicating that the capacitance remained relatively stable during cooling from 77 K to 4 K. Consequently, no significant change in the transmission coefficient behavior was expected upon cooling to 4 K. The observed increase in $\delta_{CR,4}$ by more than an order of magnitude therefore points to changes in the characteristics of the refrigerator's coaxial lines. These changes cause a shift of several dB across the entire frequency response of the total transmission coefficient. As our modeling confirmed, such a broadband shift results in a significant change in the $\delta_{CR,4}$ value. In contrast, a change in capacitance alone affects this value to a much lesser extent, as it only alters the shape of the response in a localized frequency region rather than shifting the entire characteristic.

Acularly large deviation was observed for the GRM 120 pF capacitor, which is not thermally stabilized. For this component, the relative deviation of the $S21$ parameter was 0.25554 — significantly higher than for the other capacitors. A similar trend is evident in the low-frequency data. As Table 2 shows, the nominal value of the GRM 120 pF capacitor deviated by more than 95 % at 4 K.

This substantial change in capacitance causes a pronounced shift in the frequency response of the transmission coefficient within the measured range, thereby increasing the $\delta_{CR,4}$ value.

The $\delta_{LR,4}$ results for the inductors show that the scattering matrix parameters measured at 4 K also changed significantly relative to the room-temperature values across the operating frequency range (up to 1 GHz). The relative deviations of the $S21$ parameter increased to 0.05307 for TN and 0.05196 for HQ. This change in $\delta_{LR,4}$ suggests modifications in the properties of both the measurement lines and the samples themselves, which could be due to variations in the inductance value and the characteristics of the sample holder and refrigerator lines. According to Table 6, the deviation in inductance value reached over 20 % at 4 K, doubling the deviation observed when cooling from 77 K. It is important to note that for an inductance of approximately 800 nH, a 20 % variation strongly implies that the primary influence on the measured behavior is the alteration of the measurement lines' characteristics. Furthermore, the substantial rise in $\delta_{LR,4}$ could also indicate changes in the refrigerator's coaxial cables, leading to a significant shift in the overall frequency response. Such a broadband shift, as with the capacitors, has a major impact on the $\delta_{LR,4}$ value. The presence of these significant changes in the measurement lines' parameters complicates the determination of the precise inductance variation at 4 K using this technique. In a cryogenic probe station, more precise measurements that eliminate the influence of the coaxial lines and sample holder would be required.

## Conclusion

The measurements of surface-mounted capacitors at cryogenic temperatures revealed that NPO-type and thin-film capacitors exhibited minimal capacitance deviation at 4 K, not exceeding 4 %. Consequently, their scattering matrices also showed only minor changes. The scattering matrix data obtained at 77 K and 4 K indicate that the manufacturers' provided matrix data can be reliably used for designing cryogenic UHF devices. In contrast, capacitors fabricated with non-thermally-stabilized ceramics suffered a significant loss of capacitance at cryogenic temperatures. Measurements of thin-film, surface-mounted inductors showed a 10 % change in inductance when cooled to 77 K. However, at 4 K, the pronounced changes in both the scattering matrix parameters and the inductance values — primarily influenced by the measurement lines — prevented the accurate quantification of the intrinsic inductance shift using this technique. To isolate the component's behavior, further studies in a cryogenic probe station are required to eliminate the influence of the input and output lines.

### Funding

This study was funded by the Ministry of Science and Higher Education of the Russian Federation (project № FSUN-2023-0007).

### Conflict of interest

The authors declare that they have no conflict of interest.

## References


[1] M. Schmidt, M. von Helversen, M. López, F. Gericke, E. Schlottmann, T. Heindel, S. Kück, S. Reitzenstein, J. Beyer. J. Low Temp. Phys., **193**, 1243 (2018). DOI: 10.1007/s10909-018-1932-1

[2] N. Oukhanski, M. Grajcar, E. Il'ichev, H.-G. Meyer. Rev. Sci. Instrum., **74**, 1145 (2003). DOI: 10.1063/1.1532539

[3] N. Wadefalk, A. Mellberg, I. Angelov, M.E. Barsky, S. Bui, E. Choumas, R.W. Grundbacher, E.L. Kollberg, R. Lai, N. Rorsman, P. Starski, J. Stenarson, D.C. Streit, H. Zirath. IEEE Trans. Microwave Theory Tech., **51** (6), 1705 (2003). DOI: 10.1109/TMTT.2003.812570

[4] A.V. Gordeeva, V.O. Zbrozhek, A.L. Pankratov, L.S. Revin, V.A. Shamporov, A.A. Gunbina, L.S. Kuzmin. Appl. Phys. Lett., **110**, 162603 (2017). DOI: 10.1063/1.4982031

[5] S. Weinreb, J. Bardin, H. Mani, G. Jones. Rev. Sci. Instrum., **80**, 044702 (2009). DOI: 10.1063/1.3103939

[6] J. Clarke, F.K. Wilhelm. Nature, **453**, 1031 (2008). DOI: 10.1038/nature07128

[7] G. Wendin. Rep. Prog. Phys., **80**, 106001 (2017). DOI: 10.1088/1361-6633/aa7e1a

[8] B.I. Ivanov, M. Grajcar, I.L. Novikov, A.G. Vostretsov, E. Il'ichev Tech. Phys. Lett., **42** (4), 380 (2016). DOI: 10.1134/S1063785016040076

[9] M.J. Gong, U. Alakusu, S. Bonen, M. Dadash, L. Lucci, H. Jia, L. Gutierrez, W. Chen, D. Daughton, G.C. Adam, S. Iordanescu, M. Pasteanu, N. Messaoudi, D. Harame, A. Muller, R. Mansour, S. Voinigescu. In: *IEEE Radio Frequency Integrated Circuits Symposium* (RFIC, Boston, MA, USA, 111, 2019), DOI: 10.1109/RFIC.2019.8701847

[10] B. Patra, M. Mehrpoo, A. Ruffino, F. Sebastiano, E. Charbon, M. Babaie. IEEE J. Electron Devices Society, **8**, 448 (2020). DOI: 10.1109/jeds.2020.2986722

[11] F. Teyssandier, D. Prêle. In: *Ninth International Workshop on Low Temperature Electronics — WOLTE9* (Jun 2010, Guaruja, Brazil, 2010)

[12] H. Homulle, S. Visser, B. Patra, E. Charbon. Rev. Sci. Instrum., **89**, 014703 (2018). DOI: 10.1063/1.5004484

[13] I.L. Novikov, D.I. Volkhin, A.G. Vostretso In: *IEEE 3rd International Conference on Problems of Informatics, Electronics and Radio Engineering* (PIERE) (Novosibirsk, Russian Federation, 300, 2024), DOI: 10.1109/PIERE62470.2024.10804918

[14] AVX capacitors ACCU-P series. Datasheet. URL: https://datasheets.kyocera-avx.com/Accu-P.pdf

[15] Kemet capacitors CBR series. Datasheet. URL: https://content.kemet.com/datasheets/KEM_C1030_CBR_SMD.pdf

[16] Murata capacitors GJM series. Datasheet. URL: https://www.murata.com/en-us/products/capacitor/ceramiccapacitor/overview/lineup/smd/gjm#anchor-2

[17] Murata capacitors GRM series. Datasheet. URL: https://www.murata.com/en-global/products/capacitor/ceramiccapacitor/overview/lineup/smd/grm

[18] Murata inductors. Chip coil (chip inductor) for Consumer equipment & Industrial equipment LQP03TN02 Reference specification. URL: https://search.murata.co.jp/Ceramy/image/img/P02/JELF243C-0015.pdf

[19] Murata inductors Chip coil (chip inductor) for Consumer equipment & Industrial equipment LQP03HQ02 Reference specification. URL: https://search.murata.co.jp/Ceramy/image/img/P02/JELF243C-0021.pdf

[20] B.I. Ivanov, D.I. Volkhin, I.L. Novikov, D.K. Pitsun, D.O. Moskalev, I.A. Rodionov, E. Il'ichev, A.G. Vostretsov. Beilstein J. Nanotechnol., **11**, 1484 (2020). DOI: 10.3762/bjnano.11.131

[21] D.I. Volkhin, I.L. Novikov, A.G. Vostretsov In: *IEEE 24th International Conference of Young Professionals in Electron Devices and Materials* (EDM) (Novosibirsk, Russian Federation, 800, 2023), DOI: 10.1109/EDM58354.2023.10225128